Magnetoelastic octahedral breathing mode in the ferrimagnetic La_2CoIrO_6 double perovskite

Sanghyun Lee,[1] Min-Cheol Lee,[2,3] Yoshihisa Ishikawa,[1,4] Ping Miao,[1,4] Shuki Torii,[5] C. J. Won,[6] K. D. Lee,[6] N. Hur,[6] Deok-Yong Cho,[7,*] and Takashi Kamiyama[1,4,5,†]

[1]*Institute of Materials Structure Science, KEK, Tokai 319-1106, Japan*
[2]*Center for Correlated Electron Systems, Institute for Basic Science, Seoul 08826, Korea*
[3]*Department of Physics and Astronomy, Seoul National University, Seoul 08826, Korea*
[4]*Sokendai (The Graduate University for Advanced Studies), KEK, Tokai 319-1106, Japan*
[5]*J-PARC Center, KEK, Tokai 319-1106, Japan*
[6]*Department of Physics, Inha University, Incheon 22212, Korea*
[7]*IPIT and Department of Physics, Chonbuk National University, Jeonju 54896, Korea*

(Received 3 July 2018; revised manuscript received 24 August 2018; published 6 September 2018)

Distortion of transition-metal ion-oxygen octahedra in perovskite structure has been a long standing subject for exploring the physics of charge-orbital–spin-lattice couplings. Recent findings in nickelates or $BaBiO_3$ have suggested that a charge disproportionation in the transition-metal ions can evoke certain cooperative breathing distortions (CBD), constituted by the symmetric expansion and shrinkage of the octahedra in contrast to the Jahn-Teller-type asymmetric distortion. A double perovskite ferrimagnet, La_2CoIrO_6 bears inherently the charge disproportionation in the cationic sites with Co^{2+} and Ir^{4+} sublattices. In light of seeking the clues for the CBD and its coupling to the magnetic order, the crystal structure and magnetic structure of La_2CoIrO_6 were examined at various temperatures by using neutron diffraction. Structure refinements and mode decomposition analyses revealed that, indeed, a CBD mode exists substantially in La_2CoIrO_6 while preserving the symmetry of the lattices ($P2_1/n$) and the magnetism [$\Gamma_1(A_g)$]. And more importantly, the magnitude of the symmetric distortion is correlated strongly with the size of the magnetic moment at temperatures below the Curie temperature ($\sim$95 K). This strongly suggests a magnetoelastic coupling of the CBD mode. The order parameters for CBD, e.g., the movement of O1 toward Ir ions at low temperatures, are found to be in a linear-quadratic relationship with the value of the magnetic moment ($\sim 0.002\,\text{Å}/\mu_B{}^2 M_{Co}{}^2$), manifesting the magnetoelastic CBD in double perovskite.

DOI: 10.1103/PhysRevB.98.104409

I. INTRODUCTION

Perovskite-type transition-metal oxides have been widely studied in condensed-matter researches since there have been observed a variety of emergent phenomena including, for instance, colossal magnetoresistance, multiferroicity [1], and photocatalysis [2]. In most cases of the perovskite oxides, such functionalities originate from a complex interplay among charge, orbital, spin, and lattice degrees of freedom of *d* electrons [1]. Therefore, it is of significant interest to identify the possible orders in those degrees of freedom and their correlation.

In the case of perovskites ABO_3 (typically, A is an alkali-metal or rare-earth ion and B is a transition-metal ion), the corner-sharing BO_6 octahedra can be distorted or rotate cooperatively depending on the sizes of A and B ions, which is well characterized by the Goldschmidt tolerance factor [1] and 15 Glazer tilting systems [3–6]. The most well-known type of the octahedral distortion is the Jahn-Teller distortion, that is, BO_6's are distorted asymmetrically (like an elongation in one B-O bond direction) as in $LaMnO_3$ [7] or $La_{0.75}Ca_{0.25}MnO_3$ [8].

On the other hand, certain octahedral distortion that can preserve symmetry in BO_6's has been also observed in some materials having charge inhomogeneity. For instance, alternatingly mixed Bi^{3+} and Bi^{5+} ions (rather than Bi^{4+}) in $BaBiO_3$ (Fm-3m) resulted in doubling of all the lattice constants of the aristo-type cubic ABO_3 (Pm-3m) [9], and the charge disproportionation $2Ni^{+3} \rightarrow Ni^{+3+\Delta} + Ni^{+3-\Delta}$ in $RNiO_3$ (R: rare-earth ions except La) induced a structural evolution from $Pbnm(a^-a^-c^+)$ to $P2_1/n(a^-a^-c^+)$ [10–12]. The two B ions with distinct oxidation numbers are not identical so that a cooperative expansion shrinkage of the BO_6 pair, called the cooperative octahedral breathing (CBD) mode, is allowed crystallographically.

The CBD mode can be more prevalent in a double perovskite of $A_2BB'O_6$ [Fm-3m ($a^0a^0a^0$)] [6,13–16] since B and B' sites are now fundamentally distinct. Thus the double perovskite system can be an ideal playground for exploring and controlling the CBD modes. Since the discovery of the half-metallic ferrimagnet Sr_2FeMoO_6 [17], double perovskites with various compositions have been synthesized and characterized in light of enhancing the magnetism for spintronics applications [14]. Regarding the CBD, Solovyev pointed out that the atomic position of the oxygen ions can affect the ferrimagnetism in the double perovskites of Sr_2FeMoO_6 and Sr_2FeReO_6 [18]. Also, a Raman

*zax@jbnu.ac.kr
†takashi.kamiyama@kek.jp

spectroscopy study substantiated an A_{1g} mode (related to the dynamics of the CBD-type vibration) in contrast to an E_g mode (related to the dynamics of Jahn-Teller-type vibration) in Ba_2FeReO_6 [19]. However, precise determination on the atomic positions and the information on the mode decomposition in regard to CBD are still lacking.

This paper reports precise information on the cooperative octahedral distortion/rotation in La_2CoIrO_6 obtained by time-of-flight (t.o.f.) neutron powder diffraction. This material is a ferrimagnet with an antiferromagnetic coupling between Co spins ($S_{Co} = 3/2$; Co^{2+} $3d^7$, high-spin configuration) and Ir pseudospins ($J_{eff,Ir} = 1/2$; Ir^{4+} $5d^5$) and the Curie temperature (T_C) is ~95 K [20–27]. It was shown that the octahedrally coordinated Co^{2+} with a high-spin configuration as in CoO can have a substantial unquenched angular moment, implying strong spin-orbital-lattice coupling [28]. Furthermore, the octahedrally coordinated Ir^{4+} with strong spin-orbit entanglement effect (J_{eff}-ness) as in the representative iridates of Sr_2IrO_4 [29] or Na_2IrO_3 [30] can induce exotic Kitaev-Heisenberg magnetism [30] rather than the classical Néel-type antiferromagnetism as in Li_2MnO_3 [31]. Therefore, possible magnetoelastic (ME) effects can be maximized under the composition. Indeed, we found a signature of strong positive correlation between the CBD mode and the magnetic moment in the composition. Many studies on iridate compounds have been reported, but here we report on the ME coupling with magnetic long-range order in an iridate compound.

II. EXPERIMENTAL METHODS

A La_2CoIrO_6 powder sample was prepared by solid-state reaction method [23]. The t.o.f. neutron powder diffraction was carried out on ~4 g of the specimen in the SuperHRPD beamline in J-PARC [32,33]. As shown in the Supplemental Material [34], the 90-deg bank in the end station of the beamline can collect the data with the Q value up to $Q_{max} = 10.5\ \text{Å}^{-1}$, high enough to study the ME coupling; the errors in the Ir-O bond length are displayed in Fig. S3 in comparison to previous structural studies [20,24].

The space group and lattice structures are directly determined from the t.o.f. values of the diffraction patterns from the 90-deg bank data. The atomic coordinates and the bond information, e.g., Ir-O bond lengths or Co-O-Ir bond angles, were obtained by processing the Rietveld refinement using Fullprof [35]. For the magnetic structure analyses, the data were collected from the 30-deg bank and the symmetry analyses were performed employing the SARAh program [36]. The crystal symmetry remained as $P2_1/n(a^-a^-c^+)$ for all the temperature range, while the details in the atomic positions and spin orders vary with temperature. The complex evolution in the atomic positions under $P2_1/n$ $(a^-a^-c^+)$ symmetry was interpreted in terms of the tilting and distortion of the IrO_6 and CoO_6 octahedra compared to the case of aristo-type Fm-$3m$ $(a^0a^0a^0)$ by using the Bilbao crystallographic server [37,38] and ISODISPLACE [39]. (See Ref. [34] for more details.)

III. RESULTS

Figure 1 shows the crystal structure and magnetic structure of La_2CoIrO_6 at $T = 23$ K determined by neutron powder diffraction. It is shown that the crystal structure possesses the space group of $P2_1/n$ with Glazer tilting notation of $a^-a^-c^+$ for all the T ranges below room temperature. Results of x-ray-diffraction analyses (Fig. S1 in Ref. [34]) also support the assignment. Figures 1(a) and 1(b) show the top view and the perspective view of the crystal structure, respectively. Co and Ir occupy Wyckoff $2c$ and $2d$ positions respectively, both of which have two identical sites: Co atoms are at $(x, y, z) = (0, 1/2, 0)$ and $(1/2, 0, 1/2)$, and Ir atoms are at $(x, y, z) = (1/2, 0, 0)$ and $(0, 1/2, 1/2)$. A possible antisite disorder replacing B(Co) with B'(Ir) ions was considered in the Rietveld refinement. By adding one more parameter of mixing ratio, the goodness of the fit was improved but only slightly; the R_{wp} value is reduced from 5.35 to merely 5.08% for a 9% mixing of Co ↔ Ir. Thus we judge that the effects of such antisite disorder are negligible in this compound, as is consistent with a previous report [20].

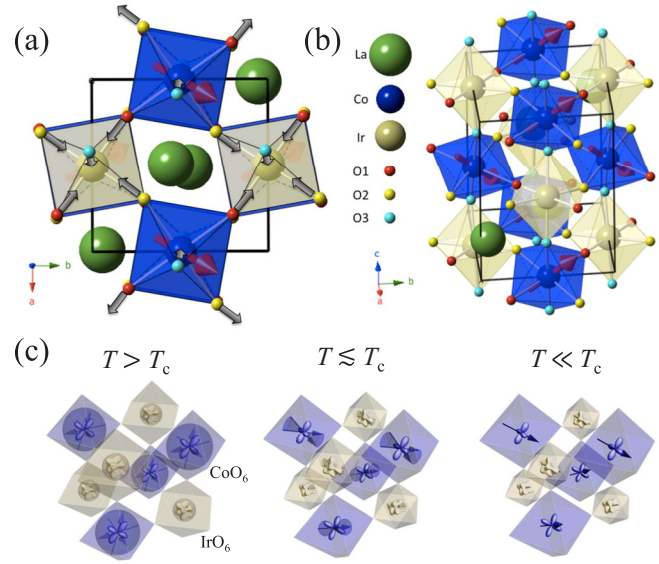

FIG. 1. (a) Top view and (b) perspective view of $P2_1/n(a^-a^-c^+)$ crystal structure and $\Gamma_1(A_g)$ magnetic structure in ferrimagnetic La_2CoIrO_6 at $T = 23$ K determined by neutron powder diffraction. The magnetic moment of Co was estimated to be $M_{Co} = (A_x, F_y, A_z) = (1.0, 1.7, 1.4)\mu_B$ while that of Ir was indeterminate ($|M_{Ir}| < 0.5\,\mu_B$). The arrows in panel (a) highlight the expansion of CoO_6 and shrinkage of IrO_6 due to ferrimagnetism at low temperature. (c) Schematic of the orbitals and spins in the networks of CoO_6 and IrO_6 octahedra. The CBD modes becomes enhanced with decreasing $T (T > T_C \rightarrow T \lesssim T_C \rightarrow T \ll T_C)$, suggesting magnetoelastic effects in La_2CoIrO_6.

The magnetic propagation vector k was estimated to be (0, 0, 0), indicating that the magnetic unit cell is identical with the crystal unit cell. The magnetic basis vectors according to the magnetic symmetry analysis are summarized in Table I. There are two possible magnetic models under the magnetic propagation vector group of $2/m$. One is $\Gamma_1(A_g)$, which dictates that if a Co ion has a magnetic moment of (M_x, M_y, M_z) (each of the components is defined as the projection to the lattice vector a, b, or c) the other Co ion in the same unit cell should have a moment of $(-M_x, M_y, -M_z)$; that is, the components of the two Co ions along the a or c axis should be

TABLE I. Symmetry analysis of $A_2BB'O_6$ double perovskite (space group $P2_1/n$) with a magnetic propagation vector $k = (0\,0\,0)$. In $P2_1/n$ symmetry, B (Co) and B' (Ir) occupy Wyckoff $2c$ and $2d$ positions, respectively. The only possible magnetic model under the magnetic propagation vector group (G_k) of $2/m$ is $\Gamma_{\rm mag} = 3\Gamma_1(A_g) + 3\Gamma_3(B_g)$ for both B and B'. The magnetic moments at B and B' are denoted by vector forms as (M_x, M_y, M_z) and (M'_x, M'_y, M'_z), respectively.

(x,y,z)	Magnetic symmetry ($G_k = 2/m$)	
	$\Gamma_1(A_g)$	$\Gamma_3(B_g)$
$B = {\rm Co}(2c)$		
$(0, 1/2, 0)$	(M_x, M_y, M_z)	(M_x, M_y, M_z)
$(1/2, 0, 1/2)$	$(-M_x, M_y, -M_z)$	$(M_x, -M_y, M_z)$
$B' = {\rm Ir}(2d)$		
$(1/2, 0, 0)$	(M'_x, M'_y, M'_z)	(M'_x, M'_y, M'_z)
$(0, 1/2, 1/2)$	$(-M'_x, M'_y, -M'_z)$	$(M'_x, -M'_y, M'_z)$

ordered antiferromagnetically, while the components along the b axis should be ordered ferromagnetically. The other model is $\Gamma_3(B_g)$, in which the two Co ions possess (M_x, M_y, M_z) and $(M_x, -M_y, M_z)$, i.e., ferromagnetic ordering along the a or c axis but antiferromagnetic ordering along the b axis. The requirement for Ir ions is the same as that for Co ions.

According to the results of the magnetic structure analyses for the low-T data, the $\Gamma_1(A_g)$ model reproduces the experimental diffraction patterns much more accurately than the $\Gamma_3(B_g)$ model (see Fig. 6). Therefore, we judge that magnetic structure in La_2CoIrO_6 has $\Gamma_1(A_g)$ symmetry. The spin alignments according to the symmetry are depicted in Figs. 1(a) and 1(b). The magnetic moment of Co ions at $T = 23$ K was estimated to be $M_{\rm Co} = (A_x, F_y, A_z) = (1.0, 1.7, 1.4)\mu_B$ so that the magnitude $|M_{\rm Co}|$ is 2.4 μ_B, ~80% of the ideal value for high-spin Co^{2+} (3 μ_B) [23].

Meanwhile, the magnetic moment of Ir ions was estimated to be much smaller ($M_{\rm Ir} < 0.5\,\mu_B$) [22] and indeterminate within the precision of the Rietveld analyses due to strong neutron absorption of Ir ions. The small value of the Ir moment possibly originates from the nature of the spin-orbital entanglement of the $J_{\rm eff}$ state in Ir^{4+} ions [40]. Namely, the expectation value of net spin/angular moment in the $J_{\rm eff}$ state would be a third of a single spin because the $j_{\rm eff} = 1/2$ state in Ir^{4+} comprises a combination of three t_{2g} orbitals with two spin-up states and one spin-down state [41]. Also, the low precision is contributed mainly by the significant neutron absorption of Ir ions [42] which reduces the magnetic peak intensities for the region of larger d's to hinder the determination of the weak Ir magnetic moments.

In fact, it can be inferred from the results of previous studies that the Ir magnetic moments ($\sim -0.38\ \mu_B$) are aligned antiparallel to the adjacent Co magnetic moments [22]. Previous bulk measurement reported that La_2CoIrO_6 undergoes a second-order magnetic transition with a single T_C [20,21,23–26]. According to the Landau theory on continuous phase transition, the single transition temperature suggests that Co and Ir sublattices should have the same magnetic irreducible representations (see Table I). Therefore, as for the magnetic

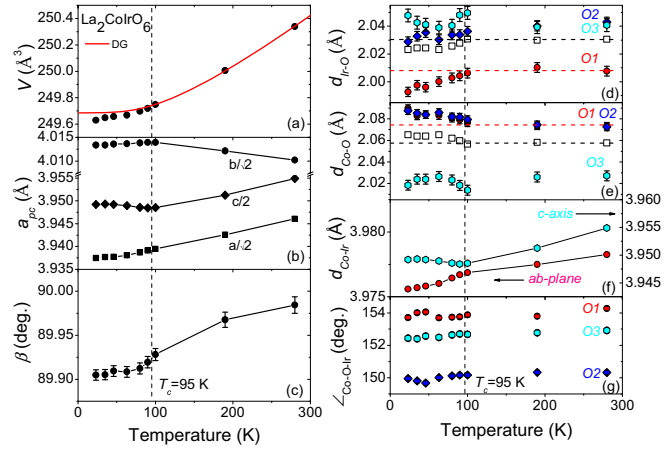

FIG. 2. (a–c) T evolutions of the lattice parameters (V, $a_{\rm pc}$, and β). The solid curve in panel (a) is the theoretical DG fit, standing for the volume expansion without magnetism. (d–g) T evolutions of the bond lengths [(d) $d_{\rm Ir\text{-}O}$, (e) $d_{\rm Co\text{-}O}$, and (f) $d_{\rm Co\text{-}Ir}$] and (g) the angles ($\angle_{\rm Co\text{-}O\text{-}Ir}$). The dashed lines in panels (d) and (e) are the guides for the eyes (high T values). All the lattice parameters and Co/Ir-O bond lengths showed a clear anomaly at T's below T_C while $d_{\rm Co\text{-}Ir}$ and $\angle_{\rm Co\text{-}O\text{-}Ir}$'s remained almost constant of T.

structure, considering the alignments of Co magnetic moments only is sufficient for identifying the magnetic structure [$\Gamma_1(A_g)$].

Examination of the atomic coordinates using the Rietveld analyses shows the correlation between the atomic positions and the ferrimagnetic order. It shows that the oxygen ions move in accordance with the Co magnetic moments as to enlarge or shrink the CoO_6 and IrO_6 octahedra cooperatively. As T decreases, the O ions in the ab plane (O1 and O2) move by ~0.02 Å toward adjacent Ir ions so as to enlarge the CoO_6 octahedra and shrink the IrO_6 octahedra, while the O ions move along c axis (O3) counteractively only by a smaller amount (<0.01 Å). (See Fig. 2 for more details.)

The mode decomposition analysis (Appendix C) shows that among the several collective oxygenic movements only the CBD mode, shown by the arrows in Fig. 1(a), is correlated with the values of the magnetic moment (mainly at T's below T_C found in Figs. 3 and 4). This suggests strong ME coupling. Namely, the CBD mode becomes severe as an increasing function of $M_{\rm Co}$ (and resultantly $M_{\rm Ir}$ as well). Figure 1(c) demonstrates the ME coupling in the networks of the CoO_6 and IrO_6 octahedra. The occupied Co t_{2g} and Ir $j_{\rm eff} = 1/2$ orbitals (lobes) and spins (arrows) are displayed schematically. The CBD modes emerge and are enhanced abruptly (but continuously) with decreasing T ($T > T_C \to T \lesssim T_C \to T \ll T_C$). At $T > T_C$, the spin directions are randomly fluctuating because the thermal energy exceeds the threshold energy of the spin order. In contrast, at $T \lesssim T_C$, the spins tend to align in their preferred orientations but with a limited coherence length, and at T's far below T_C finally all the spins reach the ground-state symmetry of $\Gamma_1(A_g)$. The orbital angular momenta would tend to align parallel or antiparallel due to the spin-orbit coupling effect, and thus the lobes appear to be perpendicular to the arrows (spins) in Fig. 1(c).

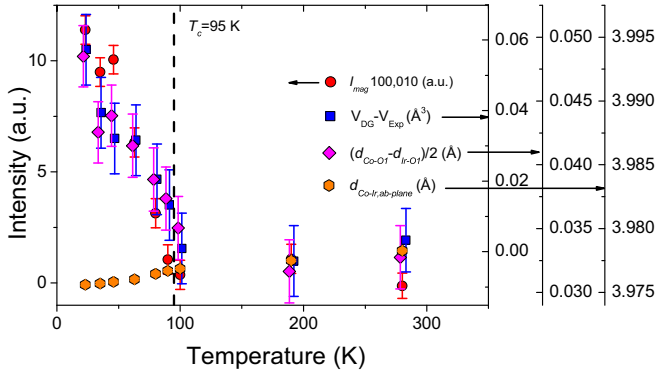

FIG. 3. Anomaly in representative order parameters: T evolution of the intensity of the (100) and/or (010) magnetic peak (I_{mag}), the volume anomaly, i.e., $\Delta V = V_{\mathrm{DG}} - V_{\mathrm{Exp}}$, and the off-center movement of O1 toward Ir [$(d_{\mathrm{Co\text{-}O1}}$-$d_{\mathrm{Ir\text{-}O1}})/2$]. Overall coincidence for all T's indicates that the structural order is strongly correlated with the ferrimagnetic order. In contrast, the variation in $d_{\mathrm{Co\text{-}Ir}}$'s is very small, implying that the magnetoelastic structural evolution is dominated by cooperative movements of oxygen ions.

The lattice parameters, bond lengths, and bond angles are displayed as functions of T in Fig. 2 and listed in Table II. The lattice parameters of (a) the unit-cell volume (V), (b) the lattice constants in a pseudocubic notation [$a_{\mathrm{pc}} = (a/\sqrt{2}, b/\sqrt{2}, c/2)$], and (c) the angle β of the monoclinic structure were determined by the t.o.f. peak positions and the systematic absence of peaks. Anomalies are shown at T's near T_{C}, suggesting a ME coupling. The theoretical Debye-Grüneisen (DG) fit is appended in Fig. 2(a) to quantitatively show the volume expansion due to thermal lattice vibrations [43,44]. It is shown that the V's at the low T's are smaller than expected by the DG fit, suggesting the shrinkage of the unit cell in accordance with the magnetic order.

Figures 2(d)–2(g) show, respectively, the bond lengths of Ir-O, Co-O, and Co-Ir ($d_{\mathrm{Ir\text{-}O}}$, $d_{\mathrm{Co\text{-}O}}$, and $d_{\mathrm{Co\text{-}Ir}}$), and the Co-O-Ir bond angles ($\angle_{\mathrm{Co\text{-}O\text{-}Ir}}$), obtained by the Rietveld refinement. The average bond lengths of ⟨Ir-O⟩ and ⟨Co-O⟩ are appended

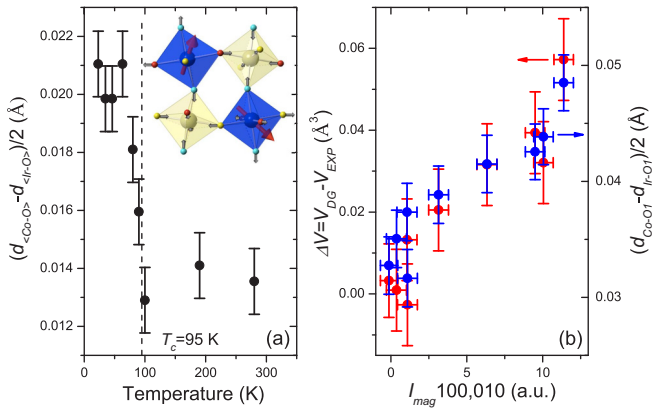

FIG. 4. (a) Difference between the average Co-O and Ir-O bond lengths [$(d_{\langle \mathrm{Co\text{-}O} \rangle}$-$d_{\langle \mathrm{Ir\text{-}O} \rangle})/2$] as a measure of CBD in the CoO_6-IrO_6 networks shown in the inset. (b) ΔV and ($d_{\mathrm{Co\text{-}O1}}$-$d_{\mathrm{Ir\text{-}O1}}$)/2's as functions of the I_{mag}'s to demonstrate the magnetism-induced CBD modes.

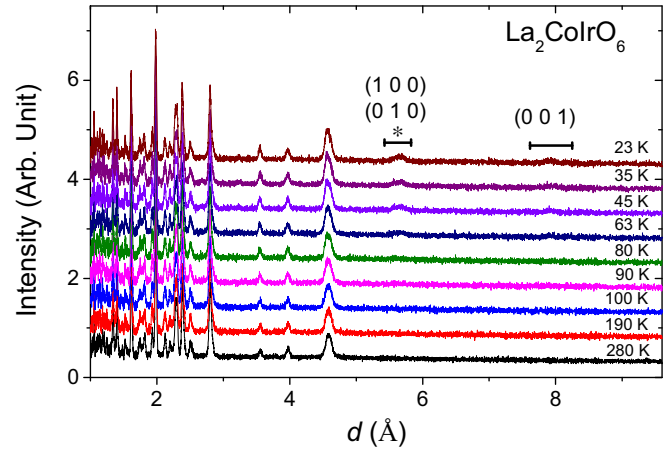

FIG. 5. Temperature evolution of the neutron powder diffraction data from the 30-deg bank.

in the respective figures. Interestingly, Ir-O bonds are shorter than Co-O bonds overall in spite of the much larger atomic number of Ir. This can be attributed mainly to the high oxidation number of Ir (+4) compared to Co (+2); the bond length decreases significantly as the electron cloud shrinks with less valence electrons.

As discussed in Fig. 1, at $T < T_{\mathrm{C}}$, Ir-O1 and Ir-O2 shrank (∼−0.02 Å) while Ir-O3 slightly elongates so that ⟨Ir-O⟩ (empty squares) decreases slightly as T decreases. In contrast, Co-O1 and Co-O2 elongate (∼+0.02 Å) while Co-O3 slightly shrank so that ⟨Co-O⟩ (empty squares) increases slightly as T decreases. Meanwhile, the Co-Ir bond lengths and Co-O-Ir bond angles barely change (<0.002 Å and <0.5°) with T, at $T < T_{\mathrm{C}}$. This suggests that O1′s and O2′s (in the ab plane) move toward adjacent Ir sites significantly whereas O3′s (along the c axis) move counteractively but only slightly. Therefore, we can infer certain collective distortion of the CoO_6 and IrO_6 octahedra.

IV. DISCUSSION

In order to scrutinize the relevance of the structural orders to the ferrimagnetic order, three representative structural order parameters are plotted together with the intensity of the "magnetic" (100)/(010) peak in Fig. 3. The (100)/(010) peaks are observed only at $T < T_{\mathrm{C}}$. (See Fig. 5). Under $P2_1/n$ crystal symmetry, the (100)/(010) reflection from nuclei is forbidden in principle. Indeed, it is not observed in the x-ray-diffraction data for all the T range (Fig. S1 in Supplemental Material [34]). Therefore, the (100)/(010) peak should originate from the magnetic scattering form factors, and their (areal) intensity I_{mag} can be regarded as a measure of strength of the magnetic ordering. The values of I_{mag}'s are obtained after subtracting the constant background around the magnetic peak.

Figure 3 shows the T evolution of the volume anomaly $\Delta V = V_{\mathrm{DG}} - V_{\mathrm{Exp}}$, that is, the magnitude of deviation from the DG fit, the off-center movement of O1 toward Ir [$(d_{\mathrm{Co\text{-}O1}}$-$d_{\mathrm{Ir\text{-}O1}})/2$], together with the values of I_{mag}'s. It is clearly shown that the two structural order parameters strikingly show a very similar T evolution to I_{mag}'s. For comparison, the distances between the cations ($d_{\mathrm{Co\text{-}Ir}}$) are attached

TABLE II. Results of the Rietveld refinement on the 90-deg bank data.

Temperature (K)	280 K	190 K	100 K	90 K	80 K	63 K	46 K	35 K	23 K
a (Å)	5.5805(1)	5.5756(1)	5.5712(1)	5.5708(1)	5.5702(1)	5.5693(1)	5.5688(1)	5.5687(1)	5.5684(1)
b (Å)	5.6713(1)	5.6740(1)	5.6766(1)	5.6765(1)	5.6764(1)	5.6762(1)	5.6760(1)	5.6758(1)	5.6758(1)
c (Å)	7.9098(2)	7.9025(2)	7.8971(2)	7.8968(2)	7.8972(2)	7.8979(2)	7.8984(2)	7.8986(2)	7.8984(2)
β (deg)	89.984(9)	89.968(9)	89.928(7)	89.919(6)	89.912(6)	89.908(6)	89.909(6)	89.905(6)	89.905(6)
V(Å^3)	250.34(1)	250.01(1)	249.75(1)	249.72(1)	249.70(1)	249.67(1)	249.66(1)	249.65(1)	249.63(1)
La x	0.5100(4)	0.5102(4)	0.5106(4)	0.5109(4)	0.5113(4)	0.5114(4)	0.5113(4)	0.5110(4)	0.5112(4)
La y	0.5503(2)	0.5512(2)	0.5520(2)	0.5524(2)	0.5522(2)	0.5524(2)	0.5527(2)	0.5526(2)	0.5527(2)
La z	0.2512(4)	0.2512(4)	0.2511(4)	0.2509(4)	0.2506(4)	0.2505(4)	0.2503(4)	0.2504(4)	0.2503(4)
O1 x	0.2112(6)	0.2104(6)	0.2108(6)	0.2111(6)	0.2114(6)	0.2122(6)	0.2128(6)	0.2131(6)	0.2131(6)
O1 y	0.2041(6)	0.2037(6)	0.2033(6)	0.2030(6)	0.2029(6)	0.2031(6)	0.2030(6)	0.2036(6)	0.2021(6)
O1 z	0.9616(8)	0.9605(8)	0.9608(8)	0.9604(8)	0.9602(8)	0.9596(8)	0.9605(7)	0.9599(7)	0.9598(7)
O2 x	0.3009(6)	0.3016(6)	0.3021(6)	0.3023(6)	0.3029(6)	0.3037(6)	0.3035(6)	0.3038(6)	0.3039(6)
O2 y	0.7045(6)	0.7046(6)	0.7054(6)	0.7058(6)	0.7054(6)	0.7055(6)	0.7048(6)	0.7050(6)	0.7058(6)
O2 z	0.9543(7)	0.9546(8)	0.9538(7)	0.9537(7)	0.9540(7)	0.9541(7)	0.9532(7)	0.9537(7)	0.9538(7)
O3 x	0.4163(4)	0.4157(4)	0.4154(4)	0.4155(4)	0.4153(4)	0.4147(4)	0.4150(4)	0.4145(4)	0.4146(4)
O3 y	0.9837(3)	0.9842(3)	0.9842(3)	0.9840(3)	0.9839(3)	0.9842(3)	0.9840(3)	0.9837(3)	0.9839(3)
O3 z	0.2509(6)	0.2509(6)	0.2524(6)	0.2518(6)	0.2512(6)	0.2509(6)	0.2512(6)	0.2513(6)	0.2520(6)
B_{iso}La(Å^2)	0.35(3)	0.24(2)	0.15(2)	0.14(2)	0.14(2)	0.12(2)	0.11(2)	0.10(2)	0.10(2)
B_{iso}Co/Ir(Å^2)	0.55(3)	0.52(2)	0.45(3)	0.45(3)	0.41(3)	0.45(3)	0.39(2)	0.42(2)	0.40(2)
B_{iso}O(Å^2)	0.63(3)	0.55(2)	0.43(2)	0.44(2)	0.45(2)	0.44(2)	0.42(2)	0.38(2)	0.40(2)
$A_x M_{Co,x}(\mu_B)$				[a]	0.3(4)	0.9(2)	0.9(2)	0.9(2)	1.0(2)
$F_y M_{Co,y}(\mu_B)$				[a]	0.8(1)	1.3(1)	1.5(1)	1.7(1)	1.7(1)
$A_z M_{Co,z}(\mu_B)$				[a]	0.8(2)	0.9(2)	1.2(1)	1.3(1)	1.4(1)
Co(μ_B)				[a]	1.2(5)	1.8(3)	2.1(2)	2.3(2)	2.4(2)
R_p(%)	4.02	4.28	4.43	4.43	4.40	4.40	4.43	4.40	4.44
R_{wp}(%)	5.35	5.75	6.05	6.06	6.04	6.03	6.04	6.03	6.10
R_{exp}(%)	2.43	2.81	2.81	2.81	2.81	2.81	2.74	2.77	2.74
χ^2(%)	4.84	4.18	4.64	4.64	4.64	4.60	4.88	4.76	4.94

[a]Values are set to zero due to too small magnetic moment below T_C.

in the figure. Compared to the case of $d_{Co\text{-}Ir}$'s, the volume anomaly and the cooperative movements of oxygen ions are found to be strongly correlated with the ferrimagnetic order. Therefore, the congruent structural anomaly at $T < T_C$ manifests the ME coupling in La_2CoIrO_6.

According to the mode decomposition analysis on the octahedral distortions (Fig. 8), there exist seven cooperative distortion modes. Among them, only the CBD mode, described in Fig. 1(c), becomes enhanced significantly with magnetic ordering at $T < T_C$. An order parameter, $(d_{\langle Co\text{-}O\rangle}\text{-}d_{\langle Ir\text{-}O\rangle})/2$, i.e., the difference between average Co-O and Ir-O bond lengths, is the most relevant to CBD. It is plotted as a function of T together with the schematic in Fig. 4(a). The correlation of the CBD mode to the magnetic order is scrutinized quantitatively in Fig. 4(b); ΔV and $(d_{Co\text{-}O1}\text{-}d_{Ir\text{-}O1})/2$ are plotted as functions of I_{mag} of the (100)/(010) reflection.

Both the order parameters show a rough linear relationship with I_{mag}'s for lower values of I_{mag}'s, whereas they seem to increase more rapidly for higher values of I_{mag}'s. Generally, intensity of magnetic peak is proportional to the squares of the magnetic moment (M^2). Therefore, the linear relationship to I_{mag} implies a linear-quadratic ME coupling (order parameters $\sim M^2$). This clearly shows the evidence of magnetoelastic CBD. The coupling constants estimated from the slopes for the low I_{mag} region are $\sim +0.002$ Å$/\mu_B{}^2 M_{Co}{}^2$ for $(d_{Co\text{-}O1}\text{-}d_{Ir\text{-}O1})/2$ and $\sim +0.008$ Å$^3/\mu_B{}^2 M_{Co}{}^2$ for ΔV.

The mechanism of the linear-quadratic magnetoelastic CBD can be demonstrated phenomenologically by the Landau free-energy scheme subject to the magnetic symmetry group. The ferrimagnetic order at $T < T_C$ breaks the time-reversal symmetry as to lower the magnetic space group from $P2_1/n1'$ to $P2_1/n$ (see Table III for comparison of the two groups). The free energy for the ME coupling compatible with the symmetry requirement can be constituted by a power series expansion of representative order parameters multiplied by the magnetic moments of Co and Ir:

$$F_{ME} = a_1(\Delta_{Co/Ir\text{-}O1})M_{Co}M_{Ir} + b_1(\Delta_{Co\text{-}Ir})M_{Co}M_{Ir} + a_2(\ldots)(M_{Co}M_{Ir})^2 + b_2(\ldots)(M_{Co}M_{Ir})^2\ldots, \quad (1)$$

where $\Delta_{Co/Ir\text{-}O1}$ and $\Delta_{Co\text{-}Ir}$ are $(d_{Co\text{-}O1}\text{-}d_{Ir\text{-}O1})/2$ and $d_{Co\text{-}Ir}(T)\text{-}d_{Co\text{-}Ir}$ (280 K), respectively, and a_1, a_2, b_1, b_2, etc., are some constant coefficients. The results in Fig. 2 show that

TABLE III. The character table for $P2_1/n1'$ for the paramagnetic phase and $P2_1/n$ (the time-reversal symmetry is broken) for the ferrimagnetic phase.

Magnetic point groups	1	2_y	-1	m_y	$1'$	$2_y1'$	$-1'$	m_y1'	Relevant parameters
$2/m1'$	1	1	1	1	1	1	1	1	$\Delta d_{Co/Ir\text{-}O}$, $\Delta d_{Co\text{-}Ir}$
$2/m$	1	1	1	1	-1	-1	-1	-1	M_{Co}, M_{Ir}

$\Delta_{\text{Co-Ir}}$ is negligible compared to $\Delta_{\text{Co/Ir-O}}$ (i.e., the CBD mode) in La_2CoIrO_6. Also, the second-order transition with single T_C dictates that the magnitude of M_{Ir} can be presumed to be proportional to that of M_{Co} : $M_{\text{Ir}} \approx -\alpha M_{\text{Co}}$. Therefore, the free energy can be simplified as the power series of ${M_{\text{Co}}}^2$ as

$$F_{\text{ME}} = c_1(\Delta_{\text{Co/Ir-O1}}){M_{\text{Co}}}^2 + c_2(\ldots){M_{\text{Co}}}^4 + \ldots, \quad (2)$$

with coefficients c_1, c_2, etc. From the condition for minimizing F_{ME}, it can be shown that $\Delta_{\text{Co/Ir-O}} \propto {M_{\text{Co}}}^2$ roughly. In fact, the linear-quadratic relationship holds in most cases of simple ME coupling. Then the rapid increase of $\Delta_{\text{Co/Ir-O1}}$ shown at high I_{mag}'s might reflect the effects of the higher-order terms in F_{ME} under strong ME effect.

Despite the significance of the ME effect, multiferroicity could not be induced in the La_2CoIrO_6 double perovskite because of the inversion symmetry of the $\Gamma_1(A_g)$ magnetic structure. All the components in the ME tensor ${\alpha^T}_{ij}$'s in $P_i = {\alpha^T}_{ij} H_j$ (where P and H are electric polarization and external magnetic field, respectively) must be zero [45,46]. Also, Song *et al.* observed no hysteresis of dielectric constant with respect to the applied magnetic field [25], supporting the absence of ferroelectric polarization in the absence of H.

The microscopic origin of the magnetoelastic CBD is unclear at this moment. One plausible explanation can be found in the hybridization mechanism for the spin interactions in double perovskite [14]. According to the hybridization mechanism, preference of the ferromagnetic or antiferromagnetic coupling of spins in adjacent B and B' sites can be determined by the virtual spin hopping from the occupied B/B' orbital to the unoccupied B'/B orbital through the hybridized orbital states [14]; in the case of La_2CoIrO_6, the occupied orbital is Ir ($j_{\text{eff}} = 1/2$) and the unoccupied orbital is Co $t_{2g}\downarrow$ [27].

It was shown in Fig. 4 that the CBD was promoted as to decrease (increase) the Ir-O (Co-O) bond length. Such changes in bond lengths can enhance the Co-Ir orbital hybridization via intervening oxygen. Thus, the inter-site spin correlation could be stronger so as to stabilize the ferrimagnetism. (See Ref. [34] for more discussions.) Likewise, the magnetic order can readjust the hybridization strengths as to induce a structural evolution through the spin-orbital-lattice coupling. However, description using the hybridization mechanism might not be reliable for explaining the delicate structural evolution driven by the ME effect. Therefore, more detailed and specific models are needed to fully understand the underlying mechanism of the magnetoelastic CBD.

V. CONCLUSION

We successfully observed the cooperative octahedral distortions and their strong correlation with the ferrimagnetic ordering in La_2CoIrO_6 using ND. The detailed analyses on the CBD showed that the CBD mode evolved with T being in a linear-quadratic relation with the magnetic moment. This manifests the existence of magnetoelastic CBD in double perovskite.

ACKNOWLEDGMENTS

The neutron-diffraction experiment using the SuperHRPD beamline was carried out under general user Program No. 2015A0318 and S-type Project No. 2014S05. D.-Y.C. was supported by Basic Science Research Program through the National Research Foundation of Korea (NRF) funded by the Ministry of Education (NRF Grant No. 2018R1D1A1B07043427), and by National Research and Development Program through the NRF funded by the Ministry of Science, ICT and Future Planning (NRF Grant No. 2017K1A3A7A09016305). S.L. was supported by Japan Society for the Promotion of Science KAKENHI Grant No. JP16K17758. We appreciate M. Hagihala for helpful discussion, and M. Shioya and K. Shimizu for technical support in the beamline experiment.

APPENDIX A: NEUTRON-DIFFRACTION DATA

The endstation in the SuperHRPD beamline in J-PARC has three detector banks of 30-, 90-, and 172-deg banks. Those detector banks can cover different d or Q ranges and their resolutions are different [32,33]. The d range of the 30-deg bank is as shown in Fig. 5. The magnetic peaks are indexed by magnetic propagation vector $k = (0\,0\,0)$. The most intense magnetic peak is from (100),(010) reflections (denoted by the asterisk), which were forbidden by $P2_1/n$ symmetry.

The results of the Rietveld refinement for the ND data taken from the 90-deg bank are listed in Table II. The lattice constants and atomic positions were determined for all the temperatures, while the magnetic moments of Co were determined reliably only at temperatures below 90 K.

APPENDIX B: DETERMINATION OF MAGNETIC MODELS

As shown in Table I, the magnetic representational analysis for the $P2_1/n$ space group and $k = (0\,0\,0)$ gives $\Gamma_{\text{mag}} = 3\Gamma_1(A_g) + 3\Gamma_3(B_g)$ for each of the Wyckoff positions $2c$ (B) and $2d$ (B') in $A_2BB'O_6$. We tested $\Gamma_1(A_g) = (A_x, F_y, A_z)$ and $\Gamma_3(B_g) = (F_x, A_y, F_z)$ magnetic models for Co sublattices, and the results are shown in Fig. 6. Obviously, the $\Gamma_1(A_g)$ model fits the intensity of the (100)/(010) peak better than the $\Gamma_3(B_g)$ models. See the contrast in the region denoted by the arrow. This is consistent with the magnetic model $(A_x, 0, A_z)$ in a previous report [21]. We got the F_y components additionally. We tested the Γ_1 models with and without the b-axis moment. The magnetic R factor R_{mag} had a large value (20.4) when the b-axis moment was set as null. With the b-axis moment, R_{mag} decreased (improved) to 14.5. The magnetic structure in the Ir sublattice was hard to determine due to the small value of the Ir magnetic moment (M_{Ir}) as well as the strong neutron absorption.

Based on the $\Gamma_1(A_g)$ model, we did Rietveld analysis on the 90-deg bank data for both crystal and magnetic structures. The results are summarized in Table II. The d range and resolution of the 90-deg bank was the most suitable to this paper, considering our sample's crystallinity and the magnetic peak positions.

Interestingly, it is found that the Co spin direction is confined in the Co-O1-Ir plane as shown in Fig. 7. When viewed in the (a) [1 1 0] or (b) [1 -1 0] direction, Co and Ir positions appear to coincide and O1 does to shift from the Co or Ir position as shown in the dotted boxes in Fig. 7. The

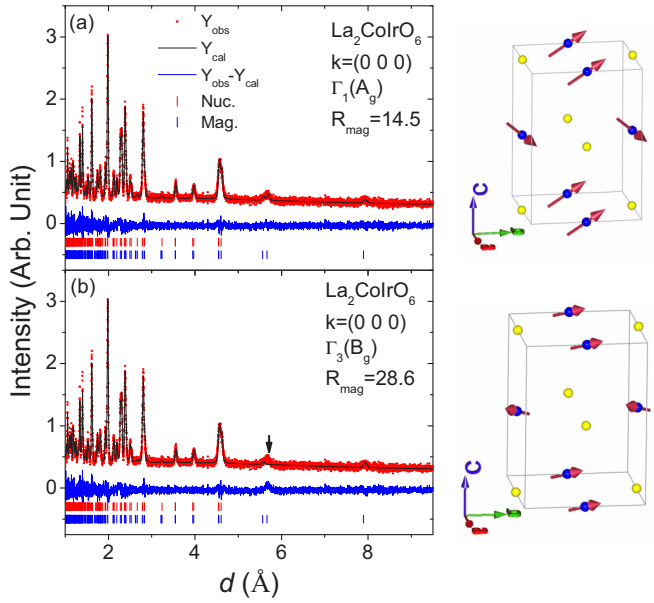

FIG. 6. Rietveld analysis using the (a) $\Gamma_1(A_g)$ and (b) $\Gamma_3(B_g)$ magnetic models for La_2CoIrO_6 at 23 K (30-deg bank data).

O1 displacements can affect both the ferrimagnetic interaction and magnetic anisotropy of the Co ions. The Co spins projected onto the (1 1 0) or (1 -1 0) planes are parallel to the directions of the O1 displacements, suggesting that the Co spins are in the Co-O1-Ir planes.

The linear-quadratic relation between the structural order parameters and the values of the magnetic moment was explained in terms of the Landau free energy. The Landau free energy is constituted by a series expansion of the order parameters multiplied by M_{Co} or M_{Ir}, that satisfies the symmetry requirements. The character table for the relevant magnetic groups is shown in Table III. The paramagnetic phase belongs to the $P2_1/n1'$ magnetic group (with time-reversal symmetry) while the ferrimagnetic phase belongs to $P2_1/n$ (time-reversal symmetry is broken). The point symmetry for $P2_1/n(1')$ is $2/m(1')$ and the character value for each of the operations is tabulated. It can be shown easily that M_{Co} or M_{Ir} can be involved in the Landau free energy only when

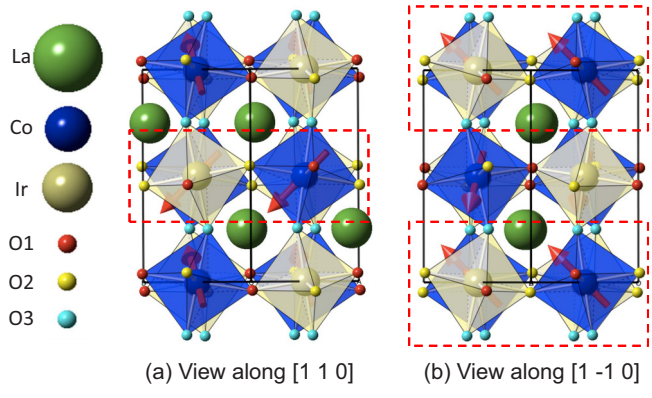

FIG. 7. Views along (a) [110] and (b) [1 -1 0]. Co spin directions are confined in the Co-O1-Ir plane.

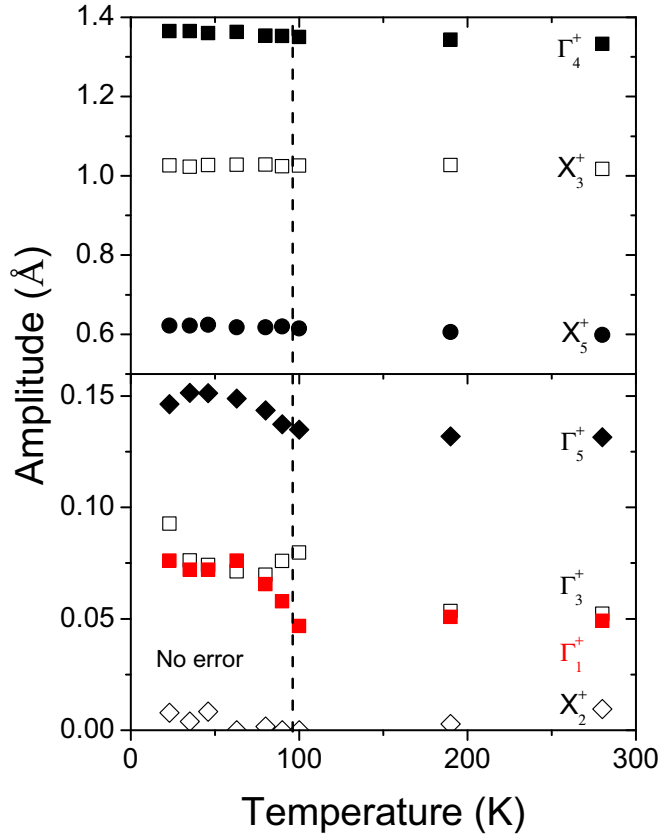

FIG. 8. Amplitudes of the seven distortion modes without error propagation. Here, Γ_1^+ distortion is the CBD mode.

it is multiplied in the even orders such as in $M_{Co}M_{Ir}$, M_{Co}^2, $(M_{Co}M_{Ir})^2$, $\Delta d_{Co/Ir\text{-}O1}M_{Co}M_{Ir}$, $\Delta d_{Co\text{-}Ir}M_{Co}M_{Ir}$, etc.

APPENDIX C: DISTORTION MODE DECOMPOSITION

As shown in Fig. S5 in Ref. [34], the octahedral distortion out of the aristo-type ABO_3 results in a lowering of crystal symmetry from $Fm\text{-}3m$ structure to the distorted $P2_1/n$ structure. Various modes on the octahedral distortions can be involved in the structural distortions. There are seven relevant distortion modes in total: Γ_1^+(CBD), Γ_3^+(a-type Jahn-Teller), $\Gamma_4^+(a^-a^-c^0$ in-plane rotation), Γ_5^+(out-of-phase bending), X_2^+(d-type Jahn-Teller), $X_3^+(a^0a^0c^+$ out-of-plane rotation), and X_5^+ (in-phase tilting). Each of the modes can be decomposed under the frozen phonon scheme in the Bilbao crystallographic server [37,38]. The values of the atomic displacements for each mode are displayed in Fig. 8. The values are also listed in Table S1 in Ref. [34].

The significance of each mode can be represented by the values of the atomic displacements in angstroms. It is shown for all T, Γ_4^+, X_3^+, and X_5^+ that distortion modes are dominant with high values of atomic displacements. This reflects the prevalence of the three distortions in La_2CoIrO_6. However, the amplitudes of the three distortion modes seem robust upon the T changes, implying they are less relevant to the ME effect.

On the other hand, Γ_1^+ and Γ_5^+ modes show strong anomalies at T's below 100 K; the two types of distortions become enhanced significantly at the low T's. The Γ_1^+ mode represents the isotropic expansion or shrinkage of the octahedral, i.e., the CBD mode. Since it shows the strongest T anomaly among the seven distortion modes, we can tell the magnetic order mainly induces the octahedral distortions mostly following the symmetry of the Γ_1^+ mode. This confirms that the CBD is associated with the magnetic order and, therefore, manifests the magnetoelastic CBD in La_2CoIrO_6.

[1] D. I. Khomskii, *Transition Metal Compounds* (Cambridge University, Cambridge, England, 2014).
[2] P. Kanhere and Z. Chen, Molecules **19**, 19995 (2014).
[3] A. M. Glazer, Acta Cryst. **B28**, 3384 (1972).
[4] C. J. Howard and H. T. Stokes, Acta Cryst. **B54**, 782 (1998).
[5] H. T. Stokes, E. H. Kisi, D. M. Hatch, and C. J. Howard, Acta Cryst. **B58**, 934 (2002).
[6] P. V. Balachandran and J. M. Rondinelli, Phys. Rev. B **88**, 054101 (2013).
[7] J. Rodríguez-Carvajal, M. Hennion, F. Moussa, A. H. Moudden, L. Pinsard, and A. Revcolevschi, Phys. Rev. B **57**, R3189(R) (1998).
[8] P. G. Radaelli, G. Iannone, M. Marezio, H. Y. Hwang, S-W. Cheong, J. D. Jorgensen, and D. N. Argyriou, Phys. Rev. B **56**, 8265 (1997).
[9] A. W. Sleight, Physica C **514**, 152 (2015).
[10] S. Catalano, M. Gibert, J. Fowlie, J. Iniguez, J-M. Triscone, and J. Kreisel, Rep. Prog. Phys. **81**, 046501 (2018).
[11] H. Guo *et al.*, Nat. Commun. **9**, 43 (2018).
[12] A. Mercy, J. Bieder, J. Íñiguez, and P. Ghosez, Nat. Commun. **8**, 1677 (2017).
[13] C. J. Howard, B. J. Kennedy, and P. M. Woodward, Acta Cryst. **B59**, 463 (2003).
[14] D. Serrate, J. M. De Teresa, and M. R. Ibarra, J. Phys.: Condens. Matter **19**, 023201 (2007).
[15] S. Vasala and M. Karppinen, Prog. Solid State Chem. **43**, 1 (2015).
[16] A. Hossain, P. Bandyopadhyay, and S. Roy, J. Alloys Compd. **740**, 414 (2018).
[17] K.-I. Kobayashi, T. Kimura, H. Sawada, K. Terakura, and Y. Tokura, Nature (London) **395**, 677 (1998).
[18] I. V. Solovyev, Phys. Rev. B **65**, 144446 (2002).
[19] A. F. Gacia-Flores, A. F. L. Moreira, U. F. Kaneko, F. M. Ardito, H. Terasita, M. T. D. Orlando, J. Gopalakrishinana, K. Ramesha, and E. Granado, Phys. Rev. Lett. **108**, 177202 (2012).
[20] R. C. Currie *et al.*, J. Solid State Chem. **116**, 199 (1995).
[21] N. Narayanan, D. Mikhailova, A. Senyshyn, D. M. Trots, R. Laskowski, P. Blaha, K. Schwarz, H. Fuess, and H. Ehrenberg, Phys. Rev. B **82**, 024403 (2010).
[22] A. Kolchinskaya, P. Komissinskiy, M. Baghaie Yazdi, M. Vafaee, D. Mikhailova, N. Narayanan, H. Ehrenberg, F. Wilhelm, A. Rogalev, and L. Alff, Phys. Rev. B **85**, 224422 (2012).
[23] M.-C. Lee, C. H. Sohn, S. Y. Kim, K. D. Lee, C. J. Won, N. Hur, J.-Y. Kim, D.-Y. Cho, and T. W. Noh, J. Phys: Condens. Matter **27**, 336002 (2015).
[24] L. T. Coutrim, D. C. Freitas, M. B. Fontes, E. Baggio-Saitovitch, E. M. Bittar, E. Granado, P. G. Pagliuso, and L. Bufaical, J. Solid State Chem. **221**, 373 (2015).
[25] J. Song, B. Zhao, L. Yin, Y. Qin, J. Zhou, D. Wang, W. Song, and Y. Sun, Dalton Trans. **46**, 11691 (2017).
[26] M. Vogl, L. T. Corredor, T. Dey, R. Morrow, F. Scaravaggi, A. U. B. Wolter, S. Aswartham, S. Wurmehl, and B. Buchner, Phys. Rev. B **97**, 035155 (2018).
[27] M.-C. Lee, S. Lee, C. J. Won, K. D. Lee, N. Hur, J.-L. Chen, D.-Y. Cho, and T. W. Noh, Phys. Rev. B **97**, 125123 (2018).
[28] S. Lee, Y. Ishikawa, P. Miao, S. Torii, T. Ishigaki, and T. Kamiyama, Phys. Rev. B **93**, 064429 (2016).
[29] B. J. Kim, Hosub Jin, S. J. Moon, J.-Y. Kim, B.-G. Park, C. S. Leem, Jaejun Yu, T. W. Noh, C. Kim, S.-J. Oh, J.-H. Park, V. Durairaj, G. Cao, and E. Rotenberg, Phys. Rev. Lett. **101**, 076402 (2008).
[30] S. M. Winter, A. A. Tsirlin, M. Daghofer, J. van den Brink, Y. Singh, P. Gegenwart, and R. Valenti, J. Phys.: Condens. Matter **29**, 493002 (2017).
[31] S. Lee, S. Choi, J. Kim, H. Sim, C. J. Won, S. Lee, S. A. Kim, N. Hur, and J.-G. Park, J. Phys.: Condens. Matter **24**, 456004 (2012).
[32] S. Torii, M. Yonemura, T. Yulius Surya Panca Putra, J. Zhang, P. Miao, T. Muroya, R. Tomiyasu, T. Morishima, S. Sato, and H. Sagehashi, J. Phys. Soc. Jpn. **80**, SB020 (2011).
[33] S. Torii, M. Yonemura, Y. Ishikawa, P. Miao, R. Tomiyasu, S. Satoh, Y. Noda, and T. Kamiyama, J. Phys.: Conf. Ser. **502**, 012052 (2014).
[34] See Supplemental Material at http://link.aps.org/supplemental/10.1103/PhysRevB.98.104409.
[35] J. Rodriguez-Carvajal, Physica B **192**, 55 (1993).
[36] A. Wills, Physica B **276**, 680 (2000).
[37] D. Orobengoa, C. Capillas, M. I. Aroyo, and J. M. Perez-Mato, J. Appl. Cryst. **42**, 820 (2009).
[38] J. M. Perez-Mato, D. Orobengoa, and M. I. Aroyo, Acta Cryst A **66**, 558 (2010).
[39] B. J. Campbell, H. T. Stokes, D. E. Tanner, and D. M. Hatch, J. Appl. Cryst. **39**, 607 (2006).
[40] C. H. Kim, H. S. Kim, H. Jeong, H. Jin, and J. Yu, Phys. Rev. Lett. **108**, 106401 (2012).
[41] C. H. Sohn, D.-Y. Cho, C.-T. Kuo, L. J. Sandilands, T. F. Qi, G. Cao, and T. W. Noh, Sci. Rep. **6**, 23856 (2016).
[42] Neutron scattering lengths and cross sections can be found in NIST database https://www.ncnr.nist.gov/resources/n-lengths/. The absorption of neutrons with the speed of 2200 m/s in Ir is 425×10^{-24} cm^2.
[43] D. C. Wallace, *Thermodynamics of Crystals* (Wiley, New York, 1972).
[44] The Debye-Grüneisen model for volume is $V = V_{0,0}(1 + \frac{E(T)}{Q - bE(T)})$. We employed the values of $V_{0,0} = 249.694$ K, $\theta_{\text{Debye}} = 457$ K, $Q = 4.6 \times 10^{-17}$ J, and $b = 1.5$.
[45] J. M. Perez-Mato, S. V. Gallego, E. S. Tasci, L. Elcoro, G. de la Flor, and M. I. Aroyo, Annu. Rev. Mater. Res. **45**, 1 (2015).
[46] A. S. Borovik-Romanov and H. Grimmer, in *International Tables for Crystallography* (Springer, Dordrecht, 2006), Vol. D, Chap. 1.5, pp. 105–149.